Detection of Prostate Abnormality within the Peripheral Zone Using Grey Level Distribution

Andrik Rampun [1], Paul Malcolm [2], and Reyer Zwiggelaar [1]

[1] Department of Computer Science, Aberystwyth University, Aberystwyth, UK

[2] Department of Radiology, Norfolk and Norwich University Hospital, Norwich, UK

Email:{yar, rrz}@aber.ac.uk, paul.malcolm@nnuh.nhs.uk

Abstract—**Development of CAD systems for detection of prostate cancer has been a recent topic of research and remains a challenging task. In this paper, we propose a novel method of prostate cancer detection within the peripheral zone. The key idea is to assume that every grey level could be associated with malignant or normal tissues by using a weighted probability. Based on the weighting, we use specific metrics to determine abnormality. We show experimental results to illustrate the performance of this method in comparison to some previous studies. Initial results show that our method achieved 81% correct classification result and 9% and 10% false positive and false negative results, respectively (sensitivity/specificity: 0.85/0.72).**

Index Terms—**prostate cancer detection, computer aided detection, histogram analysis, grey level distribution, prostate abnormality**

I. INTRODUCTION

With an estimate of 1.7 million cases globally by 2030 [1], prostate cancer is one of the most common cancers affecting men, and is a leading cause of mortality in males [2]. In 2013, there were approximately 280,000 and 40,000 cases in the United State and United Kingdom, respectively [1]. Clinical diagnostic tools such as prostate-specific antigen (PSA) level, digital rectal examination (DRE), transrectal ultrasound (TRUS) and biopsy tests are used globally despite their inconsistent results (0.51-0.89 and 0.67-0.87 sensitivity and specificity, respectively) [3]. Some of these methods are invasive and patients can suffer stress from false-positive test results, subsequent evaluation, therapy, and "over-treatment" [2].

Prostate magnetic resonance imaging (MRI) has the potential to improve the accuracy of clinical diagnostic tests [4]. Therefore the main goal of our research is to develop computer aided diagnosis (CAD) tools towards the detection of prostate abnormalities. Since 80-85% of the cancers arise within the peripheral zone [5], the proposed method only considered abnormalities that occur within this region. There have been several studies which used only the peripheral zone of the prostate [6]-[8] and allowed us to compare our quantitative results to these previous studies. Fig. 1 shows an example of

prostate MRI image with its ground truth delineated by an expert radiologist and Fig. 2 shows a schematic overview of a prostate containing a tumor.
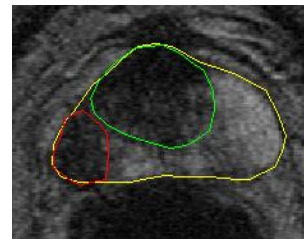

Figure 1. The ground truth of prostate gland, central zone and tumor and represented in red, yellow and green, respectively.
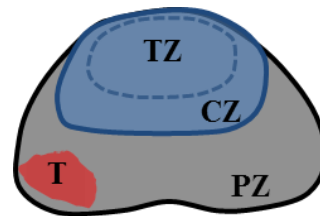

Figure 2. CZ=central zone, PZ=peripheral zone, TZ=transitional zone, T=tumor.

The proposed method compares grey level histograms from each slice with models (e.g. normal and malignant histograms models) which were constructed based on training data the distribution of grey level. Subsequently, we use specific metrics to determine abnormality. There are several methods in the literature which have used histogram analysis techniques [9]-[12]. A method proposed in [9] characterised each suspicious region of interest by performing histogram analysis on multiparametric MR images. On the other hand, [10] used colour channel histograms to capture the pattern of malignancy tissues in Gleason graded images. Moreover, [11] reports that features based histograms can achieve high sensitivity and specificity which is similar to some other features such as Gray Level Co-occurrence matrix (GLCM) and Grey Level Run-Length matrix (GLRLM). Finally, [12] used T2-weighted signal intensity histogram skewness as one of their features in differentiating between malignant and normal tissues. In terms of using grey level properties in detecting abnormalities, several studies have been done in medical image analysis application. The authors in [13] proposed a method for

recognition of lung abnormalities based on four different templates describing typical geometry and grey level distribution of lung modules [13]. On the other hand, Yu [14] proposed a method which is relying on spatial grey level dependence for detecting and locating brain abnormality. Finally, the authors in [15] proposed a method using the distribution of grey level variations for abnormality detection in mammography.

In this paper we propose a new method for detecting prostate cancer within the peripheral zone using the distribution of grey levels. In comparison to the existing methods (detecting prostate cancer in medical images) in the literature, our method is different in the sense that we do not rely on texture features such as blobs and statistical features. The methods in [16], [17] and [18] used texture features to classify malignant and normal tissue. Secondly, our method uses a single modality (T2-Weighted MRI) unlike the method in [19], which used multimodality, i.e. diffusion MRI and MR Spectroscopy. Similarly, the method proposed in [9] used multiparametric MR, i.e. T1- and T2-weighted imaging. Finally, the proposed method is purely based on the grey levels information whereas the method in [9] used additional clinical diagnostic information such as biopsy tests in deciding whether cancer is truly present or not.

II. Modelling the Peripheral Zone

Since the proposed method only considers malignant tissues/regions within the PZ, it is important to define the PZ region. We use a simple method proposed in [20], [21] which uses a quadratic equation $y = ax^2 + bx + c$ to define the boundary of PZ based on three vertex coordinates v_1, v_2 and v_3 (which can be found based on the prostate's boundary). Fig. 3 shows an example how the PZ region is defined. The coordinates of v_1, v_2 and v_3 can be determined based on the Cp (central coordinate), minimum and maximum x and y coordinates (x_{min}, y_{min}, x_{max} and y_{max}). A detailed description of the method can be found in [20], [21].
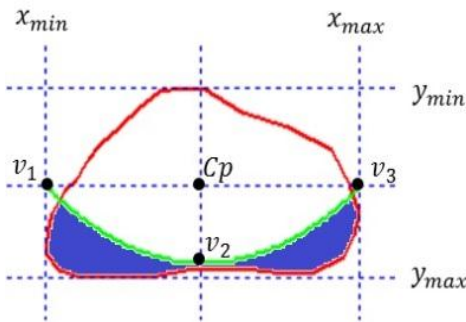

Figure 3. Prostate gland (red) and the defined PZ (indigo region) and its boundary (green) which goes through v_1, v_2 and v_3.

III. Methodology

Fig. 4 shows the overview of the proposed algorithm. In summary, the methodology relies on the distribution of grey level within the histograms which were constructed based on the grey level occurrence within 44 malignant and normal regions. The histogram models represent the

weighting values for every grey level. Based on the constructed histograms (88 slices) for each new slice, the histogram will be compared with the histogram models constructed in the early phase (yellow region in Fig. 4).
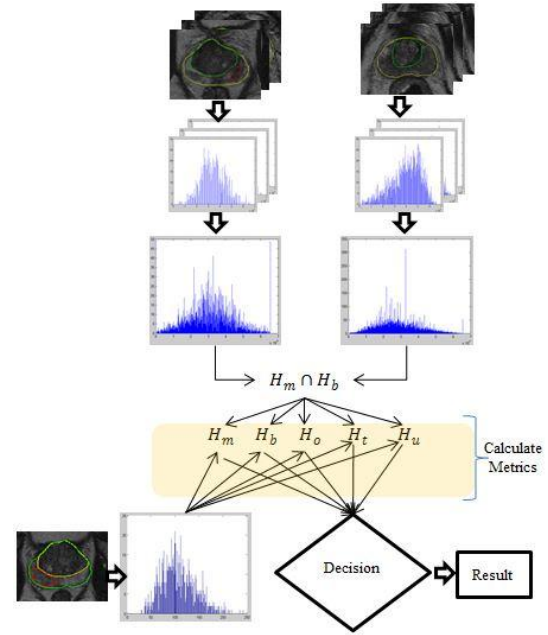

Figure 4. The overview of the proposed methodology

A. Construction of Histograms

For every slice, the proposed method constructs the first histogram (H_m) by taking every pixel intensity within the malignant region (note that all malignant regions were delineated by an expert radiologist) and each pixel is classified according to its intensity into an appropriate grey level. The second histogram (H_b) is constructed using the same process with H_m but taking normal regions instead. Normal regions are taken from the whole PZ region (with condition there is no tumors found within the PZ) as shown in Fig. 3 indigo region. This means H_m and H_b containing the distribution of malignant and normal grey level, respectively. Since every image size is 16 bits, there is a total of 65, 536 grey. There were 44 malignant and normal regions (in total 88 regions) taken from 44 slices (in total 88 slices all from 20 patients) to construct H_m and H_b. Mathematically, this process can be presented in (1), (2), (3) and (4).

$$m_n = \{i_1, \ i_2, \ i_3 \ldots i_n\} \quad (1)$$

$$b_n = \{i_1, \ i_2, \ i_3 \ldots i_n\} \quad (2)$$

$$H_m = \{m_1 + \ m_3 + \cdots + m_n\} \quad (3)$$

$$H_b = \{b_1 + b_2 + b_3 + \ldots + b_n\} \quad (4)$$

where n, i, m and b represent the nth region (or grey level), every grey level, malignant and normal region, respectively. This means, there are 44 histograms in total from 44 malignant slices (another 44 histograms from normal slices). Finally, we combine all histograms using (3) and (4) to produce the resulting models. Fig. 5 illustrates an example of this process.
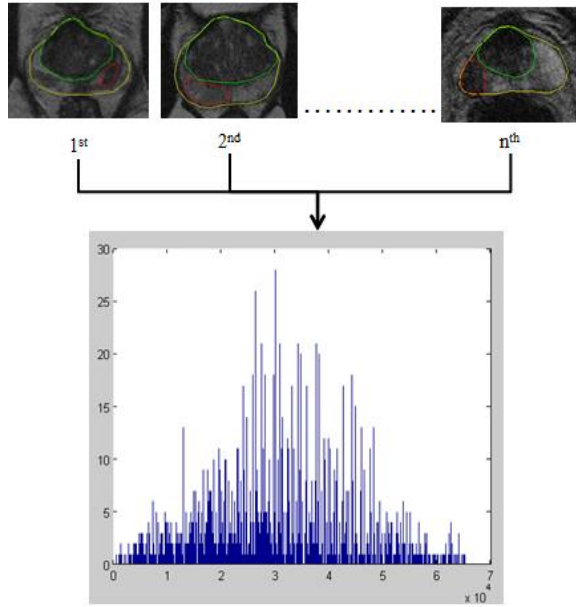
Figure 5.   An example of histogram result (H_m). The x and y axis represent the grey level location and the frequency of occurrence for every grey level.

Fig. 5 shows an example of the construction of H_m based the n slices (in our case 44 slices). Note that the pixel intensities are only taken within the malignant region which is within the red boundary in Fig. 5. The process is similar when constructing H_b but taking the PZ region as defined in Fig. 3. To this point we have constructed two histogram models which are H_m and H_b where both histograms store the frequency of grey level occurrence from malignant and normal regions, respectively. However, since many grey levels occur in both regions, we need to identify the distinctive grey levels which occur only in malignant or normal regions, and grey levels that occur both in malignant and normal regions. These allow us to differentiate malignant and normal grey tissues. These can be found by finding the intersection of H_m and H_b as shown in (5). In our case, intersection means a particular grey level can be found in both malignant and normal regions (i.e. grey level at the position 3990th occurs in H_m and H_b, see Fig. 9).

$$H_o = H_m \cap H_b \qquad (5)$$

where H_o is the histogram contains all the grey levels occur both in malignant and normal regions. Each grey level's frequency in H_o is the mean of corresponding frequencies in H_m and H_b (e.g. $H_o(i) = (H_m(i) + H_b(i))/2$) with condition that the element (i) is in H_m and H_b. Fig. 6 shows an illustration of this process in a Van diagram. From the van diagram, we can see that H_m and H_b, have their unique grey levels. The values in H_o represents grey levels 3, 50, 234 and 941 occur in both H_m and H_b. This means, prostate tissues which are fall in these grey level values are classified as malignant or normal.
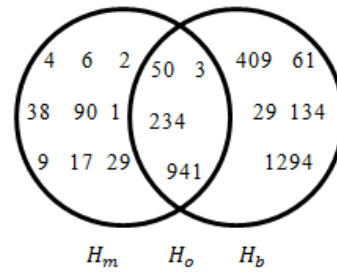

Figure 6. H_o contains all the overlap grey levels from H_m and H_b. Each element in the Van diagram represents the grey level.

By the end of this phase, we have three histogram models which present the only malignant (H_m), only normal (H_b) and malignant and normal (H_o) grey levels. Fig. 7 and Fig. 8 show examples of malignant and normal grey level distributions from grey level 38,000 to 39,000, respectively. We chose only 1000 grey levels in the following examples so the differences are visible.
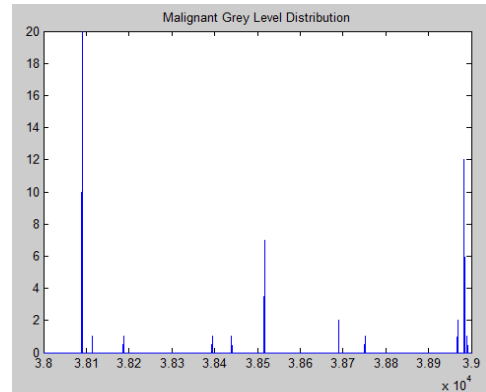

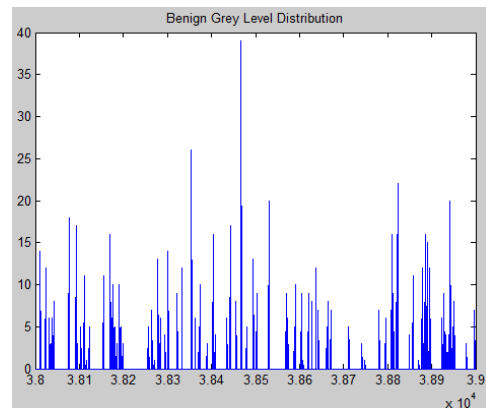Figure 7.   Malignant grey level distribution for 1000 grey levels.

Figure 8.   Normal grey level distribution for 1000 grey levels

On the other hand, Fig. 9 shows an example of grey level distribution of H_o for the same 1000 grey levels.

Based on the examples in Fig. 7-Fig 9, we can clearly see that normal regions have higher occurrence within this range and very small occurrence for malignant grey levels within this range. However, it is possible that all grey levels in malignant regions only occur in H_o (e.g. if all grey levels occur in H_o we need further steps to determine abnormality). To reduce this problem we need

to extract two more histograms from H_o. Both histograms (H_t and H_u) represents the distribution of overlapping malignant and benign grey levels, respectively. In contrast to H_o, H_t and H_u were constructed based on the exact number of occurrence of grey levels whereas H_o is based on the average occurrence number of grey levels of H_m and H_b. Therefore, every grey level now has a weighted value and using these histogram models (H_m, H_b, H_o, H_t and H_u) we could estimate the probability of abnormality using specific metrics.
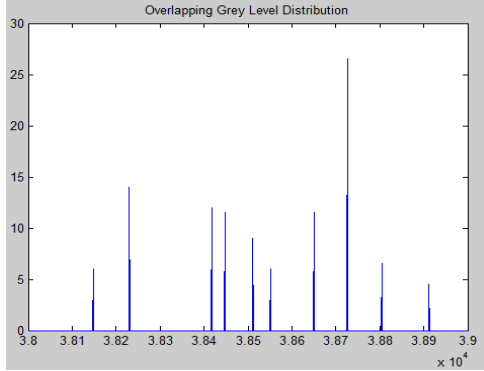

Figure 9.   Grey level distribution for **H_o**.

B. Histogram Normalisation

Since the sum of H_b outweighs considerably high the sum of H_m and H_o (caused false negative results), all models need to be normalised to ensure the weighting values for all grey levels are distributed evenly (used for the first metric only). By normalising all histogram models the sum for every histogram is equal to 1. The normalisation can be done using the following equation

$$h_k(i) = \frac{H_k(i)}{\sum H_k(i)} \qquad (6)$$

where $k \in \{m, n, o, t, u\}$ and h (small h) indicates a normalised histogram. Therefore we get an equal summation of histogram but still different distributions and weighting value for every grey level's location.

C. Abnormality Detection

In the proposed method, abnormality detection is performed by calculating specific information from every histogram which is extracted from PZ. We use the following metrics to measure abnormality.

- The sum of histogram multiplication ($H_{j\times k}$) for each H_j with each of h_k (e.g. h_m and h_b). This can be calculated using the following equation

$$H_{j\times k} = \sum_{j=1} H_j(i) \times h_k(i) \qquad (7)$$

This metric indicates the product of probability when every element in H_j is multiplied with every element (frequency) in h_k. This means, the higher the value of $H_{j\times k}$ the more chance the slice has a tumor. For instance, $H_{j\times m} > H_{j\times b}$ means the malignant product of probability is higher when multiplied with h_m compared to h_b. A large number of $H_{j\times m}$ indicates there are many grey

levels in H_j have the same grey level in h_m (similar case in $H_{j\times b}$ and $H_{j\times o}$).

- The histogram intersection ($H_{j\cap k}$) [22] between h_j and h_k which can be calculated using the following

$$H_{j\cap k} = \sum_{j=1} \min\{H_j(i), H_k(i)\} \qquad (8)$$

Based on (8), we do not use the normalised histograms (h_k) but H_k (denormalised histogram) instead, because normalised histograms could affect the value of histogram intersection due to the small values in h_k which lead to incorrect results. We used this metrics as it has been successfully used for similarity measure in many different applications including medical image analysis. This metric measures the closeness of match between two histograms (in our case H_j and H_k). Higher value of $H_{j\cap k}$ indicates higher probability of the histograms is similar. In the proposed method, this matric is used to measure the closeness of a match between every H_j with the histogram models. The closer the match with model the higher the value of $H_{j\cap k}$. Finally, higher value means most gray levels in both histograms are distributed equally.
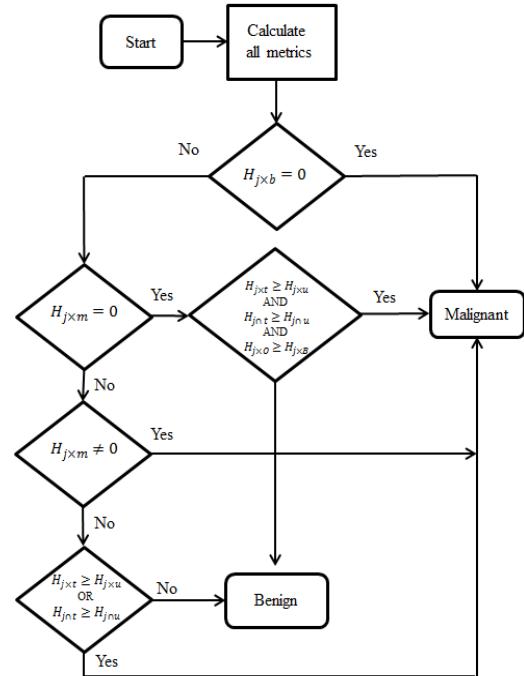

Figure 10. Flow chart decision rules.

Finally, now we have seven variables ($H_{j\times m}$, $H_{j\cap t}$, $H_{j\times t}$, $H_{j\times b}$, $H_{j\cap u}$, $H_{j\times u}$ and $H_{j\times o}$) which will be used to determine as whether abnormality is present or not based on the decision rules in Fig. 10. It should be noted that there are other metrics in the literature [23] available but these will be investigated in the future. Based on Fig. 10, it is clearly shows that if $H_{j\times m}$, $H_{j\cap t}$ or $H_{j\times k}$ value is higher than $H_{j\times b}$, $H_{j\cap u}$ or $H_{j\times u}$ indicates higher

probability of the prostate being abnormal. Similarly when the prostate's slice is more likely to be benign, the values of $H_{j \times b}$, $H_{j \cap u}$ or $H_{j \times u}$ are greater than $H_{j \times m}$, $H_{j \cap t}$ or $H_{j \times k}$. In the next section we will present our experimental results.

IV. EXPERIMENTAL DATA

In this study, we used 243 slices of T2-Weighted MRI images taken 35 different patients aged 47 to 79. The data contains 88 slices of training data from 20 patients and 50 % of the training data are malignant and the other half is normal. For evaluation purpose we used 155 slices of MRI images from 35 patients and 105 slices of them are malignant and 50 slices are normal. Our data were collected from Norfolk and Norwich Hospital University and for every slice all ground truths (prostate gland, central zone and tumor) were delineated by an expert radiologist.

V. EXPERIMENTAL RESULTS

This section presents the experimental results based on 155 slices T2-Weighted MRI images with 105 slices are malignant and 50 slices are normal from 35 different patients aged 49 to 74. The prostate, cancer and central zones were delineated by an expert radiologist on each of the images. Each slice was analysed and classified as to whether the prostate contains abnormality based on the methodology described in section three. Next, we compared the result with the ground truth as to whether the prostate contains cancer regions or not. An abnormality is considered to have been detected if the classification result is correct in comparison with the ground truth. We use several quantitative measures to evaluate the results such as sensitivity (Sen), specificity (Spe) and Accuracy (Acc). Each of these metrics can be calculated using the following equations

$$Sen = \frac{TP}{TP+FN} \qquad (9)$$

$$Sen = \frac{TN}{TN+FP} \qquad (10)$$

$$Acc = \frac{TN+TP}{TN+TP+FP+FN} \qquad (11)$$

where *TP* and *FP* denote the numbers of true positive and false positive, respectively. Similarly, *TN* and *FN* show the numbers of true negatives and false negatives. Accuracy means the number of correct classified slices out of the total number of slices. Sensitivity measures the proportion of actual positives which are correctly identified (in this case the percentage of malignant slice which are correctly identified) whereas specificity measures the proportion of actual negatives which are correctly identified (in this study the percentage of normal slice which are correctly identified).

The proposed method achieved 81% correct accuracy, which means 126 slices were classified correctly with 0.85 and 0.72 sensitivity and specificity, respectively. On the other hand, the proposed method produced 9% and 10% false positive and false negative results, respectively. In

comparison with existing methods in the literature the proposed method achieved similar results. Nevertheless, it is extremely difficult to make a qualitative comparison due to the differences in datasets (different modalities such as T2-weighted (T2-W) MRI, diffusion-weighted (DWI) MRI, dynamic contrast enhanced (DCE) MRI, Magnetic resonance spectroscopy (MRS), etc.) and frameworks used by the other methods. However, to compare the proposed method, we cite several methods which have similar goals (detecting prostate cancer). There are many other methods in the literature but it is difficult to gather all of those methods (also space limitation) and we selected these methods (see Table I) because they have at least one of the qualitative results (e.g. sensitivity) and it is clearly stated the number of cases used in the evaluation.

TABLE I. FROM THE LEFT COLUMN REPRESENTS THE AUTHORS, NUMBER OF PROSTATES/PATIENTS, ACCURACY RATE, SENSITIVITY, SPECIFICITY AND MODALITIES, RESPECTIVELY

Authors	#	Acc	Sen	Spe	Mod
Sung et al. [24]	42	89	89	89	DCE
Vos et al. [9]	29	89	-	-	T2-W+DCE
Ampeliotis at al. [3]	10	87	-	-	T2-W+DCE
Rampun et al. [21]	19	85	82	87	T2-W
Tiwari et al. [25]	19	84	-	-	T2-W+MRS
Artan and Yetik. [8]	15	82	76	86	DCE
Our method	35	81	85	72	T2-W
Castaneda et al. [26]	15	80	67	86	CrW
Reinsberg et al. [27]	42	-	81-93	64-73	DWI+MRS
Litjens et al. [28]	188	-	84	-	DWI+DCE
Futterer et al. [29]	6	-	83	83	T2-W
Girouin et al. [30]	46	-	78-81	32-56	T2-W
Llobet et al. [18]	303	-	57	61	Ultrasound

Table I presents the experimental results of thirteen different methods including the proposed method and their accuracy, sensitivity, specificity and modalities. All methods were ordered based on accuracy, sensitivity and specificity accordingly. Note that some of the authors did not include one/two of these qualitative results (indicated as '-'). The method proposed in [9] and [24] achieved the highest correct classification rate (89%) followed by the method in [3] with 87% accuracy. Our method has similar accuracy result with the method in [26] with just 1% higher. In addition, the proposed method reported similar sensitivity with the methods proposed in [21], [28] and [29] and the method of [24] reminds 89%. Although the method proposed in [27] achieved the highest sensitivity but the authors reported inconsistency of 81%-93%. The method in [18] achieved the lowest accuracy which is 57% whereas the method in [8] and [26] produced 76% and 67% sensitivity, respectively. On the other hand, the methods

in [21], [26], [8] and [29] achieved high specificity 87%, 86%, 86% and 83%, respectively. The proposed method achieved only 72% but it is still higher than the methods proposed in [18] and [30].

These comparisons are subjective because accuracy, sensitivity and specificity are highly influenced by the number of datasets, different modalities and methods' framework. For instance, although the method proposed in [26] and [29] achieved 86% and 83% specificity, respectively; the evaluation is based on smaller numbers of dataset (6 and 15 patients, respectively). On another study [31] shows higher sensitivity and specificity of 93% and 96%, respectively but based on 46 ultrasound images. Similarly, the method proposed in [24] and [9] achieved the highest accuracy but based on DCE and T2-W+DCE modalities, respectively. Therefore it is extremely difficult to make a direct comparison either quantitatively or qualitatively. However, for indirect comparison purpose our method achieved comparable results with the state of art. One obvious drawback of this method is since it entirely relying on the grey level distribution, the metrics could give inaccurate results if the data is heavily affected by noise (due to change of pixel intensity affected by noise).

VI. CONCLUSIONS

We have introduced a novel method for automated prostate cancer detection using grey level distribution. The proposed method achieved similar results to some of the methods in the literature. The proposed method shows that prostate abnormalities could be detected using grey level distribution by giving a weighted value (by normalising the histogram models) for each of the grey levels. Moreover, in this paper we have shown the importance of grey-level values in detecting prostate abnormality by assigning every grey level into different classes (e.g. malignant or benign) and assigning a weighting value for every single grey level's location. In short, with 9% and 10% false positive and false negative results, respectively we have achieved comparable results (81% accuracy out of 35 patients). Although it is difficult to make a quantitative comparison with the methods in Table I due the differences in datasets and frameworks, the main objective to show the potential of grey level distribution in detecting prostate cancer because it has been showed its potential in different human's body such as breast [15], lung[13] and brain[14]. Finally, the next stage of this research is to test it on a larger dataset with several combination methods [20], [21] and applying a robust noise reduction method to improve its sensitivity and specificity.

ACKNOWLEDGMENT

REFERENCES

[1] N. Howlader, A. M. Noone, *et al.* (2013). Seer cancer statistics review, 1975-2010, national cancer institute. [Online]. Avaiable: http://seer.cancer.gov/csr/1975 2010/. Accessed 16-October-2013

[2] R. Chou, J. M. Croswell, *et al.* (Oct. 2010). A review of the evidence for the U.S. preventive services task force. [Online]. Avaiable: http://www.uspreventiveservicestaskforce.org/uspstf12/prostate/prostateart.htm

[3] K. K. Yu and H. Hricak, "Imaging prostate cancer," *Radiol. Clin. North. Am.*, vol. 38, no. 1, pp. 59-85, 2000.

[4] D. Ampeliotis, A. Antonakoudi, K. Berberidis, and E. Z.Psarakis, "Computer aided detection of prostate cancer using fused information from dynamic contrast enchanced and morphological magnetic resonance images," in *Proc. IEEE International Conference on Signal Processing and Communications*, 2007.

[5] S. B. Edge, D. R. Byrd, C. Compton, A. G. Fritz, F. L. Greene, and A. Trotti, *AJCC Cancer Staging Manual,* 7th Ed. Chicago, US: Springer, 2010.

[6] H. Ito, K. Kamoi, K. Yokoyama, K. Yamada, and T. Nishimura, "Visualization of prostate cancer using dynamic contrast-enhanced MRI: Comparison with transrectal power doppler ultrasound," *Br. J. Radiol.*, vol. 76, no. 909, pp. 617-624, Sep. 2003.

[7] I. Ocak, M. Bernardo, G. Metzger, T. Barrett, P. Pinto, P. S. Albert, and P. L. Choyke, "Dynamic constrast-enhanced MRI of prostate cancer at 3T: A study of pharmokinetic parameters," *Amer. J. Roentgenology*, vol. 189, no. 4, pp. 192-200, Oct. 2007.

[8] Y. Artan and I. S. Yetik, "Prostate cancer localization using multiparametric MRI based on semi-supervisedtechniques with automated seed initialization," *IEEE Trans. Inf. Technol. Biomed.*, vol. 16, no. 6, pp. 1313-1323, 2012.

[9] P. C. Vos, T. Hambrock, J. Barentsz, and H. Huisman, "Computer-assisted analysis of peripheral zone prostate lesions using T2-weighted and dynamic contrast enhanced T1-weighted MRI," *Physics in Medicine and Biology*, vol. 55, pp. 1719-1734, 2010.

[10] A. Tabesh, V. Kumar, H. Pang, D. Verbel, A. Kotsianti, M. Teverovskiy, and O. Saidi, "Automated prostate cancer diagnosis and Gleason grading of tissue microarrays," in *Proc. SPIE Med. Imag.*, vol. 5747, Apr. 2005, pp. 58-70.

[11] M. Radhakrishnan, T. Kuttiannan, and N. Tiruchengode, "Comparative analysis of feature extraction methods for the classification of prostate cancer from trus medical images," *International Journal of Computer Sciences*, vol. 9, no. 2, 1991.

[12] Y. Peng, Y. Jiang, *et al.*, "Quantitative analysis of multiparametric prostate MR images: Differentiation between prostate cancer and normal tissue and correlation with Gleason score—A computer-aided diagnosis development study," *Radiology*, vol. 267, no. 3, pp. 787-796, 2013.

[13] A. Farag, A. El-Baz, G. G. Gimel'farb, R. Falk, and S. G. Hushek, "Automatic detection and recognition of lung abnormalities in helical CT images using deformable templates," *Lecture Notes in Computer Science*, vol. 3217, pp. 856-864, 2004.

[14] Y. M. Yu, "Detecting and locating of brain abnormality in MR images using texture feature analysis and improved probabilistic relaxation methods," *WSEAS Transactions on Biology and Biomedicine*, vol. 10, no. 2, pp. 57-66, 2013.

[15] M. Hachama, A. Desolneux, and F. Richard, "Combining registration and abnormality detection in mammography," in *Proc. International Workshop on Biomedical Image Registration; Utrecht*, The Netherland, July 9-11, 2006, pp. 178-185.

[16] E. A. Yfantis, T. Lazarakis, and G. Bebis, "On cancer recognition of ultrasound image," in *Proc. IEEE Workshop on Computer Vision beyond the Visible Spectrum: Methods and Applications*, 2000, pp. 44-49.

[17] R. M. Haralick, *et al.*, "Textural features for image classification," *IEEE Trans. on Systems, Man and Cybernetics*, vol. 3, no. 6, pp. 610-621, 1973.

[18] R. Llobet, J. C. Perez-Cortes, A. H. Toselli, and A. Juan, "Computer-aided detection of prostate cancer," *Int. J. Med. Inform.*, vol. 76, no. 7, pp. 547-556, 2007.

[19] M. R. Engelbrecht, P. Puech, P. Colin, O. Akin, L. Lemaitre, and A. Villers, "Multimodality magnetic resonance imaging of prostate cancer," *Journal of Endourology Society*, vol. 24, no. 5, pp. 677-684, 2010.

[20] A. Rampun, Z. Chen, and R. Zwiggelaar, "Detection and localisation of prostate abnormalities," in *Proc. 3rd International Conference on Computational Mathematical Biomedical Engineering*, 2013.

[21] A. Rampun and R. Zwiggelaar, "Detection of prostate abnormality within the peripheral zone using local peak information," in *Proc. 3rd International Conference on Pattern Recognition Applications and Methods*, 2014.

[22] Overlapping histograms. [Online]. Available: https://sites.google.com/site/daishizuka/toolkits/overlapping-histograms

[23] S. H. Cha, "Comprehensive survey on distance/similarity measures between probability density functions," *City*, vol. 1, no. 2, pp. 300-307, 2007.

[24] Y. S. Sung, H. J. Kwon, *et al.*, "Prostate cancer detection on dynamic contrast-enhanced mri: Computer-Aided diagnosis versus single perfusion parameter maps," *American Journal of Roentgenology*, vol. 197, no. 5, pp. 1122-1129, 2011.

[25] P. Tiwari, J. Kurhanewicz, M. Rosen, and A. Madabhushi, "Semi supervised multi kernel (sesmik) graph embedding: Identifying aggressive prostate cancer via magnetic resonance imaging and spectroscopy," in *Medical Image Computing and Computer-Assisted Intervention–MICCAI 2010*, Springer, 2010, pp. 666-673.

[26] B. Castaneda, L. An, *et al.*, "Prostate cancer detection using crawling wave sonoelastography," in *Proc. SPIE Medical Imaging: Ultrasonic Imaging and Signal Processing*, 2009.

[27] A. Reinsberg, G. S. Payne, *et al.*, "Combined use of diffusion-weighted MRI and 1H MR spectroscopy to increase accuracy in prostate cancer detection," *American Journal*, vol. 188, no. 1, pp. 91-98, 2007.

[28] G. J. S. Litjens, P. C. Vos, J. O. Barentsz, N. Karssemeijer, and H. J. Huisman, "Automatic computer aided detection of abnormalities in Multi-Parametric prostate MRI," in *Proc. SPIE Medical Imaging: Computer-Aided Diagnosis*, 2011.

[29] J. J. Futterer, *et al.*, "Prostate cancer localization with dynamic contrast-enhanced mr imaging and proton mr spectroscopic imaging," *Radiology*, vol. 241, no. 2, pp. 449-458, 2006.

[30] N. Girouin, *et al.*, "Prostate dynamic contrast-enhanced mri with simple visual diagnostic criteria: is it reasonable?" *European Radiology*, vol. 17, no. 6, pp. 1498-1509, 2007.

[31] A. Wong and J. Scharcanski, "Fisher–tippett region-merging approach to transrectal ultrasound prostate lesion segmentation," *IEEE Transactions on Information Technology in Biomedicine*, vol. 15, no. 6, pp. 900-907, 2011.

Andrik Rampun received his B.Sc. and M.Sc. in Software Engineering from MARA University of Technology, Malaysia and Hertfordshire University, UK in 2008 and 2011, respectively. He is currently a second year PhD student at the Department of Computer Science, Aberystwyth University, UK. His current research interests are Prostate Imaging particularly in abnormality detection and localisation as well as Texture Based Segmentation. On the other hand, he is also interested in e-learning on social networks.

Paul Malcolm received a BSc in Biochemistry and basic medical sciences in 1983 from Kings College, London and qualified in Medicine from the University of London in 1986. He is a fellow of the Royal College of Radiologists and currently a consultant radiologist and research lead in radiology at the Norfolk & Norwich University Hospital, UK. His clinical interests include imaging of prostate cancer and his research interests are in new MRI techniques for measurement of body compartments and function.

Reyer Zwiggelaar received the Ir. Degree in Applied Physics from the State University Groningen, Groningen, The Netherlands, in 1989, and the Ph.D. Degree in Electronic and Electrical Engineering from the University College London, London, UK, in 1993. He is currently a Professor at the Department of Computer Science, Aberystwyth University, UK. He is the author or co-author of more than 180 conference and journal papers. His current research interests include Medical Image Understanding, especially Focusing on Mammographic and Prostate Data, Pattern Recognition, Statistical Methods, Texture-Based Segmentation, and Feature-Detection Techniques.